ACS OMEGA

Open Access

http://pubs.acs.org/journal/acsodf

Article

Aminoglycoside/Hexadecanoic Acid Complex Lamellar Core Nanoparticles

Ajay J. Khopade* and Nitin Chitranshi

Cite This: *ACS Omega* 2024, 9, 50766−50773

Read Online

ACCESS | Metrics & More | Article Recommendations

ABSTRACT: An aminoglycoside, tobramycin sulfate (TbS), was complexed with hexadecanoic acid (HdA), resulting in a TbS/HdA complex with a repeat unit of 5.3 nm of a lamellar nanostructure. The nanometer-sized TbS/HdA particles were produced using poloxamer 188 as a dispersing agent. The particles were agglomerate-free with sizes in the range of 90−450 nm. The particle size was controlled by optimizing the homogenization conditions and the concentration of poloxamer-188. The lamellar nanostructure of the TbS/HdA complex was retained in the nanoparticle cores, even after the rigorous homogenization step. These core−shell-type nanoparticles were called lamellosomes because each particle consisted of a TbS/HdA lamellar core surrounded by a crown of hydrophilic poloxamer. The ζ-potentials of nanoparticles were in the range of −20 to −26 mV and did not aggregate even after exposing them up to the concentrations of 0.2 mol L^{-1} NaCl. However, the nanoparticles were sensitive to the changes in the pH in terms of their aggregation or disintegration. Thus, the steric effects and ionic charge seem to be responsible for the stabilization of the nanoparticles. The TbS/HdA matrix or HdA lamella could dissolve dexamethasone up to ∼2% (w/w) without causing crystallization. The release of the entrapped drug was significantly retarded. The TbS/HdA lamellosomes could serve as aminoglycoside carriers, which can further load drugs, showing potential as a multidrug cargo.

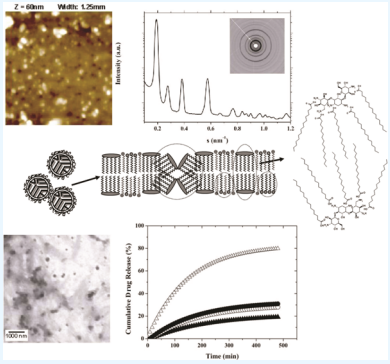

INTRODUCTION

The charged polyelectrolyte can interact with oppositely charged surfactants to produce materials such as core−shell nanoparticles, vesicles, and thin films that can be used for a variety of applications such as drug delivery, cell models, and corrosion resistance.[1,2] However, the cationic surfactants or polyelectrolytes can cause severe cytotoxicity[3] and hence are either not used in drug delivery applications or very low concentrations; for example, a polycationic polyelectrolyte Polyquad and a cationic surfactant benzalkonium chloride are used in the range of 0.005% (w/w) to 0.04% (w/w) in pharmaceutical applications. This limitation is overcome by using polycationic saccharides such as aminoglycoside (AmG) antibiotics, which are USFDA-approved therapeutically active compounds against bacterial infections. Their polycationic nature makes them suitable candidates for designing colloidal drug delivery systems through interaction with oppositely charged (anionic) surfactants.[4] The conjugation of hydrophobic groups to the AmG hydrophilic core targeting rRNA led to the development of amphiphilic broad-spectrum antibacterial AmGs that constitute a new class of antibiotic agents acting on bacterial membranes.[5] The AmG-based colloidal systems can be an alternative to be used for sustained ophthalmic, pulmonary, or intravenous drug delivery and improved absorption through the gastrointestinal tract to improve the overall therapeutic efficacy.

Tobramycin sulfate (TbS) is an AmG antibiotic that is widely used in pharmaceutical eye drops and inhalation solutions. All five amino groups of AmG remain ionized at low pH, providing them with the maximum charge density. They can form several different ionic complexes, for example, with metal ions[6] and anionic polyelectrolytes (PEs).[7,8] PE/TbS multilayer capsular systems have shown excellent biocompatibility and suitability for ophthalmic use. The primary mechanism of their antibiotic action is the interaction of anionic lipids of cell membrane and immediate disruption.[9] Based on the same principle, this work is extended to the formation of polycation/lipid complexes. In this paper, we report the preparation and characteristics of colloidal nanoparticles of TbS/HdA complexes. Understanding the physicochemical properties of the colloidal TbS/HdA lamellar systems will help us to evaluate their use as a sustained release ocular, pulmonary, or intravenous drug delivery system. In analogy with cubosomes and hexosomes, colloidal particles have cubic or hexagonal internal microstructures.[10] TbS/HdA systems are termed lamellosomes, as we show that the internal

Received: October 6, 2024
Revised: November 30, 2024
Accepted: December 3, 2024
Published: December 11, 2024

microstructure of TbS/HdA complex nanoparticles is lamellar. The internal lamellar structure within PE/fatty acid complex nanoparticle spheres could bear different mesomorphic structures: liposome-like structure of concentric lamellae and a structure of parallel layers due to the presence of microphase-separated combination of nonionic, ionic, and TbS-complexed species of fatty acid that can statistically present different packing parameters within the system. The term tart-type particle refers to the latter.[11] By superimposing these limiting examples, more like a "patchwork" that is of our interest can be created. Our definition of lamellosomes is restricted to the tart-type and patchwork-type microparticles consisting of lipids and lipid/PE complexes. These are different than the core−shell particles with a solid or liquid core surrounded by a shell in providing both aqueous and lipid micro- or nanomesophasic compartments within the core where either hydrophilic or lipophilic molecules can be encapsulated.

The TbS/HdA lamellosome systems may have several advantages such as an increase in the activity of the antibiotic drug due to the use of fatty acids.[12] Mariella and coauthors compared and discussed the studies on tobramycin nanocarrier systems, called nanoantibiotics, conducted over 2000−2022.[13] They concluded that repurposed tobramycin nanoantibiotics have potential to improve the efficacy after topical treatment of cystic fibrosis in lung or eye infections. The improved activity may translate into reduction of dose and side effects like lipidosis.[14,15] The colloidal TbS/HdA lamellosome systems further entrap nonpolar molecules due to the HdA component. A widely marketed combination of TbS is with corticosteroids, such as dexamethasone, loteprednol, prednisolone, and fluorometholone, which are nonpolar and hence may be incorporated in these colloidal particles, making them ideal carrier systems for the aminoglycoside−corticosteroid combination.[16] They may also be used to encapsulate other antibiotics as a part of combination therapy such as penicillins, cephalosporins, glycoprotein antibiotics, and other aminoglycosides.[17,18] The specificity of aminoglycoside toward nucleic acids may be useful in effective targeting of anticancer drugs with this system.[19] The abundance of palmitic acid in pulmonary surfactants makes colloidal TbS/HdA lamellosome systems suitable for the treatment of pulmonary infections as inhalation formulations.[20] Palmitic acid is also present in marketed lung surfactant compositions, called Survanta. This paper is yet another attempt in pharmaceutical research to create a new nanoantibiotic system for aminoglycosides by the optimization of TbS/HdA complex nanoparticles.

EXPERIMENTAL SECTION

Materials. *N*-Hexadecanoic acid (HdA) was purchased from Merck (Germany). The aminoglycoside, tobramycin sulfate (TbS), and dexamethasone (DxM) were supplied by Sun Pharma (India). Poloxamer 188 was obtained from BASF (Germany); pyrene and dilaurylcarboxyfluorescein were obtained from Sigma-Aldrich. Other chemicals and solvents used were of AR grade and were used as received.

METHODS

Preparation of Complexes. TbS (1.0 M) was dissolved in water. HdA (5.0 M) was dispersed in water by using NaOH (pH 7.0). The TbS solution was slowly added to the HdA dispersion to obtain a gel-like consistency material. The TbS/HdA gel was mixed for further 30 min at 70−80 °C and stored in glass vials for further characterization. The nanoparticles were prepared by dispersing TbS/HdA in a 0.5% (w/v) aqueous poloxamer solution using a homogenizer. The complexes were also prepared with varying TbS/HdA molar ratios. Pyrene or dilaurylcarboxyfluorescein (CF) was incorporated into the colloidal complexes by adding 0.01% (w/v) pyrene in tetrahydrofuran. The pyrene-loaded colloids were studied by fluorescence spectroscopy, and CF-loaded colloids were observed by confocal microscopy (see later). Following dye loading experiments, DxM loading experiments were conducted. For that, DxM was dissolved in a minimum amount of propylene glycol, and aliquots equivalent to 0.1−2% w/w TbS/HdA complex were added. The complexes were then dispersed into lamellosome particles as discussed before. The maximum amount of DxM that can be loaded in lamellosomes was determined by observing the particles under an optical microscope and under cross polarizers for the presence of DxM crystals.

Microscopy. The optical images were taken with a Leica TCS SP microscope. The microscope had a cross-polarizer attached to it. Images were captured at a magnification of 100× using an oil immersion objective. Atomic force microscopy (AFM) imaging was performed on a Nanoscope III Multimode SPM (Digital Instruments Inc., Santa Barbara, CA) at room temperature (20−25 °C) in a tapping mode. The silicon tips (Nanotips, DI) used had a spring constant of 40 N m^{-1} and a resonance frequency of ∼300 kHz. The force between the tip and the sample was <10 nN, and the scan rate was 0.5−1 Hz. The images were acquired in a constant force mode. NanoScope software and Image PC software were used for image processing. The measurements were done on a sample prepared on a freshly cleaved mica surface. A drop of a diluted dispersion was applied on the mica surface and dried under ambient conditions. Similarly, samples were prepared on carbon-coated copper grids for TEM measurements (Zeiss EM912 Omega microscope operated at 120 kV).

Spectral Analysis. Raman spectra were collected using a Raman microscope from WiTec (Germany), and fluorescence emission spectra were collected from 350 to 500 nm using a Fluorolog spectrophotometer with an excitation wavelength of 330 nm and slits of 5/5 nm. Turbidity was measured as a function of percentage transmission at 650 nm on a Cary 100 UV-spectrophotometer (Varian).

Particle size, ζ-Potential, and Conductivity Measurements. The particle size and ζ-potential were measured on a Malvern Zetasizer 4 (Malvern Instruments U.K.). The Zetasizer uses the Smoluchowski relation, $\zeta = \upsilon\eta/\varepsilon$, to calculate the ζ-potential. In this equation, η is the viscosity, ε is the permittivity of the solution, υ is the mobility, and ζ refers to the zeta potential of the particles. The conductivity of the solutions was measured on a conductometer (Metrohm).

X-ray Scattering Measurements. Wide-angle X-ray scattering (WAXS) measurements were performed on a Nonius PDS120 powder diffractometer. A monochromatic CuKr primary radiation beam (achieved by a curved Ge crystal) was directed to the sample. The scattered radiation was measured using a Nonius CPS120 position-sensitive detector at a 2θ resolution of 0.018°. Small-angle X-ray scattering (SAXS) measurements were carried out using an Anton Paar model A-8054 (Austria) instrument. The instrument was equipped with a X-ray vacuum camera, pinhole collimation, and image plates (type BAS III, Fuji). A MAC Science Dip Scanner (IPR-420) and an IP reader (DIPR-420) were used to read the image plates.

https://doi.org/10.1021/acsomega.4c09105
ACS Omega 2024, 9, 50766−50773

Thermal Analysis. The differential scanning calorimetry (DSC) measurements were performed on a Netzsch DSC 200 instrument (Germany). The endotherms were obtained twice by performing two heating and two cooling cycles at a scanning rate of 10 K min^{-1}. The endotherm from the second cooling cycle provided transitions of HdA and the TbS/HdA complexes.

Release Experiments. Release experiments were conducted by using a Franz diffusion cell. The sample placed in a donor compartment contained 5 mg of DxM and 15 mg of TbS. The receptor compartment was filled with a release medium consisting of PBS (pH 7.4) or PBS containing 10% ethanol maintained at 37 °C. The donor and receptor compartments were separated by a cellulose acetate membrane with 500 kD MW cut off. At various time intervals, aliquots (0.5 mL) were removed from the medium. The compartment was replaced with the same amount of the fresh medium. The amount of TbS and DxM released in the medium was determined by analyzing the samples by HPLC.

Drug Analysis. The HPLC method for TbS is reported elsewhere.[4] The method for DxM analysis is as follows: a HPLC Hypersil BDS C18 column (250 × 4.6, 5 μm) maintained at 50 °C. The mobile phase was triethylamine/acetate buffer: acetonitrile (7:3) and orthophosphoric acid sufficient to adjust the pH to 4.0. The injection sample volume was 10 μL. The mobile phase flow rate was 1 mL/min. The eluted DxM was detected by using a UV detector at 240 nm. The retention time was 12−13 min.

RESULTS AND DISCUSSION

Polarized Light Microscopy and Raman Microscopy. The chemical structures of TbS and HdA are shown in Figure 1a. In the polarized optical microscopy images of TbS/HdA complexes, birefringent oily streaks with undulations were observed (Figure 1b), indicating supramolecular structures in the complexes, typical of lamellar phases. The Raman spectra of HdA, TbS, and TbS/HdA are shown as spectra 1, 2, and 3, respectively (Figure 1c). Raman spectra of these TbS/HdA lamellar complexes show strong methylene vibration bands at 2290 cm^{-1} corresponding to HdA control. There is a presence of a carboxylic acid −OH vibration band, meaning that some of the acid functions do not form acid−base pairs and remain free. This carboxylic acid −OH vibration band disappears for the 1:1 stoichiometric ratio of TbS/HdA complexes. However, this conclusion needs more sensitive techniques such as NMR to confirm to preclude the presence of an expected partial acid−base pair in this system.

Size, ζ-Potential, and Morphology. The TbS/HdA complexes were dispersed into nanoparticles using poloxamer at different concentrations, keeping homogenization conditions the same. The colloidal particles were then analyzed for particle size, ζ-potential, and morphological characteristics. The sizes of the particles were in the range of 95−490 nm (Figure 2a). The lowest particle size was ∼100 nm, and the largest size was ∼490 nm when the poloxamer concentration was decreased from 0.5% w/w to 0.1% w/w. The PDI values were less than 0.3. There was a tailing observed toward lower particle size, most likely due to the presence of blank poloxamer and palmitic acid micelles/mixed micelles at the pH studied. The poloxamer acts as an emulsifier, resulting in smaller particle size and narrow size distribution. It also prevents fine particles from aggregating in the colloidal system. The relative standard deviation of the particle size measurements was within the range 20−30%. The ζ-potential values ranged from −15.0 ± 4.5 to −23 ± 3.0 mV at

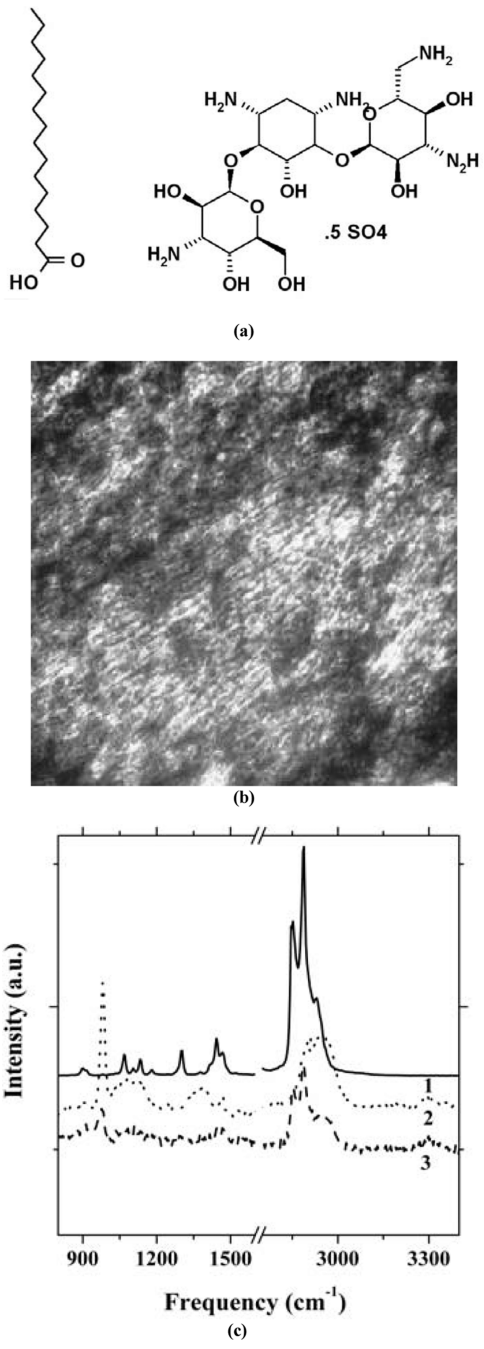

Figure 1. (a) Chemical structures of HdA (1) TbS (2), (b) polarized light microscopy image of TbS/HdA complexes showing birefringent streaks (Image width ∼100 μm), and (c) Raman spectra of HdA (1), TbS (2), and TbS/HdA complexes (3).

poloxamer concentrations of 0.1−0.5% w/v, respectively, suggesting that the particles were negatively charged, and the ζ-potential had an inverse relationship with the poloxamer concentrations due to the masking of the surface charge and the resultant reduced electrophoretic mobility. An AFM image of TbS/HdA nanoparticles is shown in Figure 2b. The width and height of the particle have a ratio of 1.8, suggesting an ellipsoidal shape due to drying. The mean size was found to be ∼95 nm. The spherical particles with a mean size of ∼100 nm were also observed under a transmission electron microscope (Figure 2c), which corroborates with that of the AFM image and the light scattering data.

https://doi.org/10.1021/acsomega.4c09105
ACS Omega 2024, 9, 50766−50773

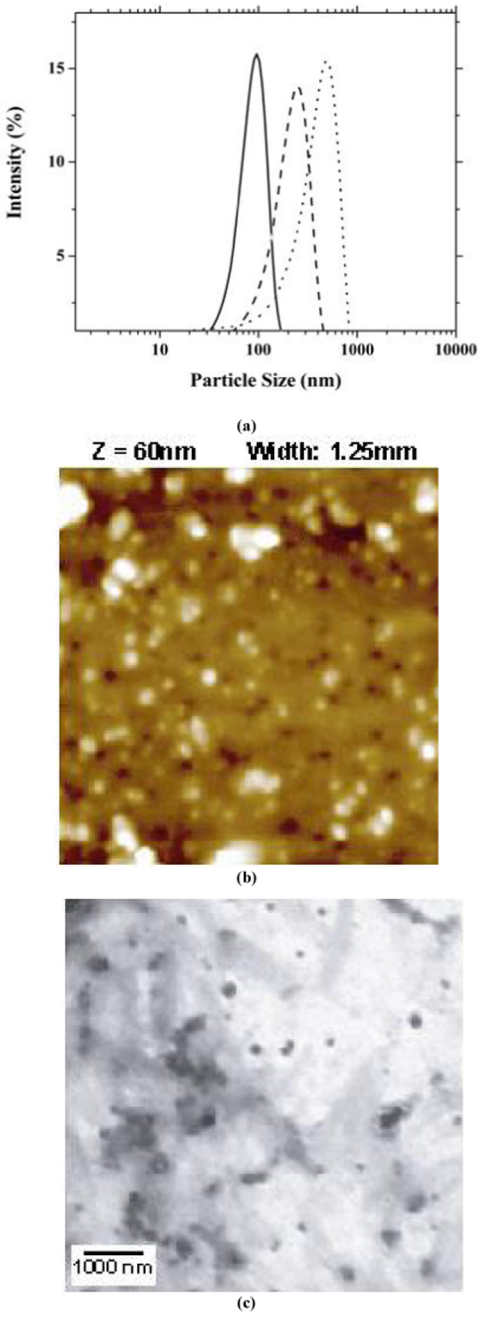

Figure 2. (a) Histogram of lamellosome particles in dispersion. Solid Line: 0.5% w/v poloxamer; dashed line: 0.3% w/v poloxamer; dotted line: 0.1% w/v poloxamer. (b) AFM image of lamellosome particles prepared with 0.5% w/v poloxamer. (c) TEM image of lamellosome particles prepared with 0.5% w/v poloxamer.

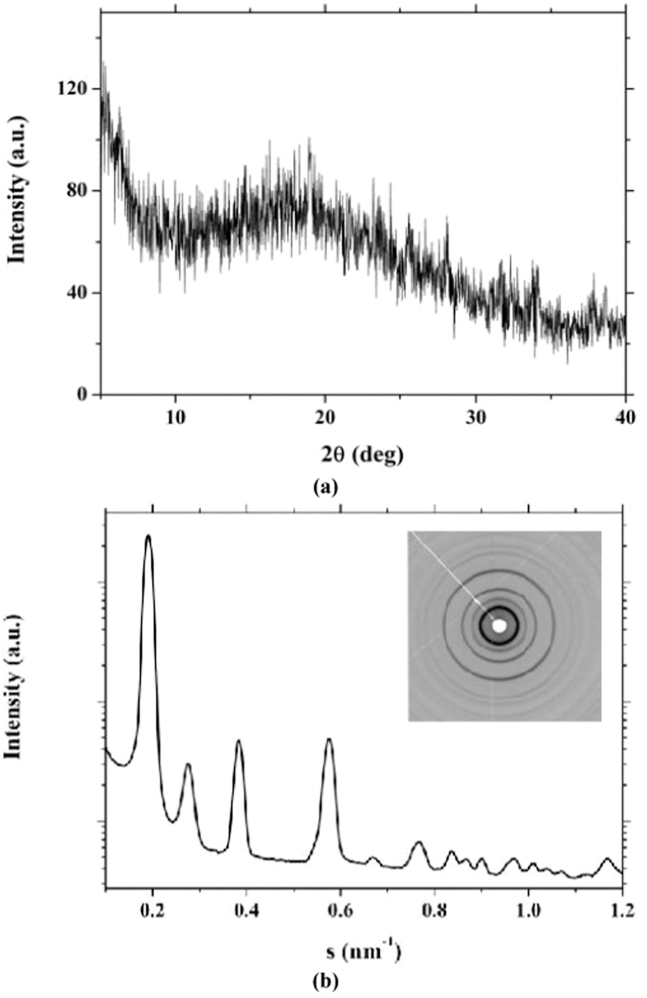

Figure 3. (a) Wide-angle X-ray scattering curve of TbS/HdA. (b) Small-angle X-ray scattering curve of TbS/HdA at pH 7.0.

Supramolecular Structures. The TbS/HdA complex nanoparticle supramolecular structure was deduced from the WAXS and SAXS measurements and their thermal properties by DSC. An example of the WAXS diagram of the TbS/HdA complex is given in Figure 3a. The wide-angle diffraction spectrum of the complex shows a broad maximum with a Bragg spacing of 0.44 nm, suggesting a liquid-like ordering of the alkyl chains in the lamellosomes. A comparison of the wide-angle diffraction spectra of the complex and the noncomplexed HdA suggests that the alkyl chains in the complexes are less densely packed than those in the free acid form (not shown). In the small-angle scattering spectrum of the aqueous suspension of the complex (Figure 3b), 3−4 peaks are present at equal distances. The peak ratio is in the order of $1:\sqrt{2}:2:\sqrt{6}:3:\sqrt{12}$... The position of the first scattering vector ($0.19\ nm^{-1}$) corresponds to a lamellar distance of 5.26 nm. A few periodic reflections are present within the primary periodic reflections corresponding to the order of 3.7 nm ($s = 0.27\ nm^{-1}$). The peaks in the order of $\sqrt{2}$, $\sqrt{6}$, and $\sqrt{12}$ (typical of the cubic phase) along with 1, 2, and 3 (typical of the lamellar phase) suggest the presence of undulation/pores arranged in a nearly cubical fashion within the lamellae. The presence of such periodic undulations of the layer surfaces is not uncommon and are also present in the cationic dendrimer/anionic lipid complex structures.[21] In our case, the TbS/HdA complex may microphase separate due to different packing parameters and may be present periodically in bilayers. The X-ray scattering characteristics of the TbS/HdA complexes at various stoichiometic ratios (1:10, 1:15, and 1:20 molar ratios) prepared at various pH (pH: 5.0, 6.0, and 7.0) were investigated. The main scattering peak position was used to determine the interlamellar distance. The interlamellar distance was found to increase with increasing pH and the HdA fraction in lamellosomes, as summarized in Table 1. At lower pH (pH 7.0), more free HdA is present, hence the interlamellar distance is lower due to bilayer packing, analogous to the presence of cholesterol phospholipid bilayers.[22] At pH 7.0, the interlamellar distance is maximum. It can be concluded that higher pH tends

https://doi.org/10.1021/acsomega.4c09105
ACS Omega 2024, 9, 50766−50773

Table 1. X-ray Scattering and Thermal Characteristics of TbS/HdA Complexes

TbS/HdA molar ratio	pH of HdA solution	lamellar distance (nm)[a]	$T_{m_{max}}$ (°C)[b]
1:10	5.0	4.65	52
1:10	6.0	5.26	33
1:10	7.0	5.71	34
1:15	7.0	5.14	27
1:20	7.0	5.0	27

[a]Calculated from the first major peak. [b]Peak of highest intensity.

to ionize HdA and increase the interlamellar distance. At a constant pH, the increase in the TbS/HdA complex reduces the interlamellar distance. At 1:1 stoichiometry (1:5 molar ratio), the lamellar distance is the least, and bicontinuous lamellae similar to those observed in a Pn3m cubic or distorted cubic phase is observed.[23] We have observed kinking, reduction of the interlamellar distance, and interconnecting sponge or foam-like vesicle formation in the phospholipid lamellae by incorporation of polycationic poly(amidoamine) dendrimer/dicetyl phosphate complexes.[20] Thus, considering the distribution of the TbS/HdA complexes and free HdA within the ionic HdA (HdA^{Θ}) lamellae, a variety of ordered supramolecular structures are possible.

The supramolecular structures of the complexes were corroborated by the thermal characteristics of the complexes studied by DSC. The endothermic transitions were found in the temperature range from 0 to 80 °C (Figure 4). These transitions

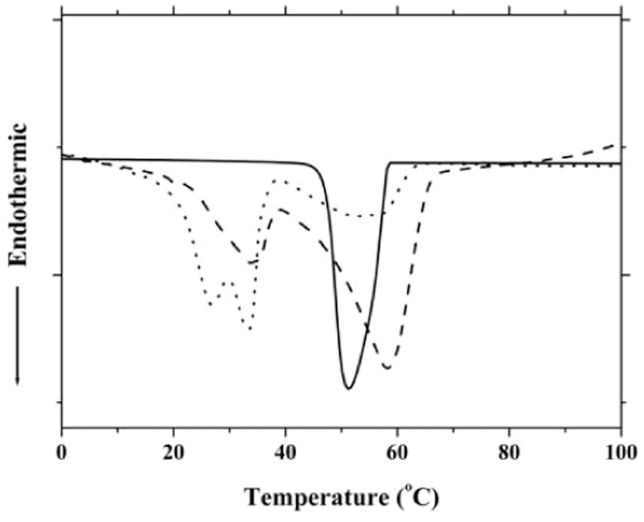

Figure 4. DSC thermograms of TbS/HdA. Solid line: HdA; dashed line: TbS/HdA complex, first heating cycle; dotted line: TbS/HdA complex, second heating cycle.

may be due to the melting of crystalline side chains of the HdA. The thermal properties of the first thermal cycle run were compared with those of the second and third cycle after the sample solidification at room temperature. Since the rate of cooling could also influence the thermogram, it was standardized for the experiment. The sample was cooled to 20−25 °C over a period of 10−15 min, and the system was equilibrated at 25 °C before repeating the heating cycle. In Figure 4, the melt transition peaks (T_m) of the TbS/HdA complex and HdA are seen, which seem to disappear in the second and third heating cycles. The second scan is more reproducible, indicating that the rearrangement of alkyl groups occurs in the TbS/HdA complex. The first cycle likely reflects the impact of sample processing, while the second and third cylces represent the behavior of different phases under standardized cooling conditions. This observation was made by Blandamer et al., explaining that the system present after the first scan is in a metastable state.[24] Two types of phases coexist within the TbS/HdA complexes, as indicated by the two peaks in the DSC thermogram. The one at the lowest temperature (~25 °C) is due to HdA^{Θ} lamellae cooperativity and the one at ~33 °C is due to TbS/HdA complexes embedded in HdA^{Θ} lamellae. An additional broad peak at 54 °C indicates the presence of a small amount of HdA in the free form. Thus, the internal lamellar structure within the PE/fatty acid complex nanoparticles contains different mesophase structures: a structure of parallel layers (lamellae), kinked layer, or periodically undulated bilayer, due to the presence of microphase-separated combination of nonionic, ionic, and TbS-complexed species of fatty acid. The finding corroborates with the SAXS study, which also indicates the TbS/HdA-doped lamellar structures. No evidence of crystallization was detected in the system under a polarized light microscope.

The thermal characteristics of the TbS/HdA complexes at various molar ratios and prepared at various pH values were also investigated. The peak position and maximum intensity peaks ($T_{m_{max}}$) were noted in the DSC thermograms. The results are summarized in Table 1. Higher pH (7.0) tends to ionize HdA, increase cooperative phase transition, and hence the maximum intensity peak is obtained at 27 °C. At lower pH (5.0), less amount of free HdA is present; hence, the peak at 52 °C is predominant. At 1:10 stoichiometry and pH 7.0, the peak at 33 °C has the maximum intensity. The lamellosome model consisting of HdA lamellae doped with a TbS/HdA complex and free HdA is consistent with the SAXS results.

Lamellosome Model. Based on the above findings, we have proposed a lamellosome model consisting of a randomly arranged lamellar phase stabilized by a poloxamer corona. This is illustrated in Figure 5. The lamellar phase consists of hydrophobic alkyl chains forming a hydrophobic planar compartment separated by planar/bicontinuous aqueous compartments consisting of TbS. The lamellae contain free HdA and the poloxamer at the surface of the lamellosome particles. HdA is shown as a cluster separately from the Tbs/HdA complex. While this mode seems to be unlikely when palmitic acid is ionized due to significant repulsion. But this scenario can be expected when HdA/Tbs exceed a 5:1 ratio. The palmitic acid pK_a is ~4.75, and full ionization is predicted at the studied pH 7. The PPO chains anchor on the particle surface and PEO chains of the triblock copolymer protrude out into the aqueous environment, providing steric stabilization of the particles like "stealth" liposomes.[25] The "stealth" functionality is shown to confer high stability and long circulation times in vivo. In the context of the proposed topical use, it may be useful in terms of reducing the irritation potential of eye drops.

Resistance to Ionic Stress and Dilution. The interaction of ionic and hydrophobic forces results in lamellosome nanoparticle formation stabilized by a nonionic block copolymer, poloxamer. Since the cores are a lamellar network, the rearrangement and aggregation of the particles are possible with the factors that affect ionic and hydrophobic interactions. The formulation is meant to be used as eye drops, and it will be exposed to tears upon instillation into the eye. Tears mostly consist of salts and electrolytes with a small quantity of proteins.

https://doi.org/10.1021/acsomega.4c09105
ACS Omega 2024, 9, 50766−50773

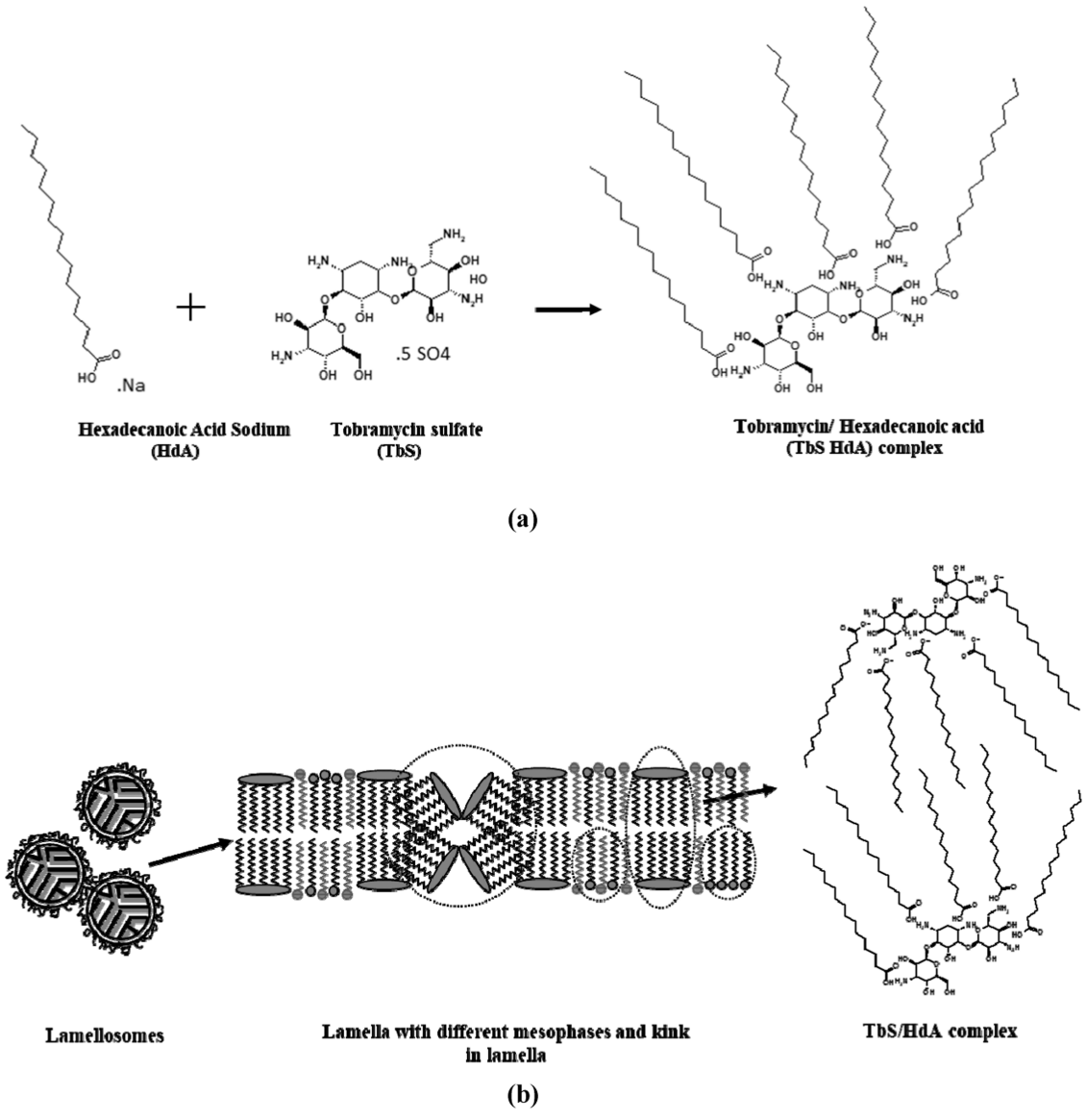

Figure 5. (a) Schematic representation of TbS/HdA complex formation. (b) Schematic representation of lamellosomes. The internal molecular structure consists of a lamellar patch-work core of TbS/HdA complexes surrounded by a poloxamer corona. Different mesophases are indicated by dotted circles. HdA is shown as a cluster separately from the Tbs/HdA complex. This mode seems to be unlikely when palmitic acid is ionized due to the significant repulsion but can be expected when TbS/HdA exceeds a 1:5 ratio.

Hence, saline (sodium chloride) is used as a biorelevant medium to study the stability of the lamellosomes as resistance to ionic stress. The resistance to ionic stress also demonstrates steric stabilization or a stealth property imparted by the poloxamer to the particles. The study was conducted by exposing TbS/HdA in 1−100 mg L^{-1} dilution to the solutions of sodium chloride of different concentrations in a stirred reactor. The turbidity (as a function of % transmission @ 650 nm), particle size, and electrical conductivity were measured. The results are presented in Figure 6a. The diameters of the nanoparticles remain unchanged up to a concentration of 0.2 mol L^{-1}, which is approximately 1.5 times that of an isotonic sodium chloride solution. The mean particle size was around 150 nm, and it remained the same for a week. The batch was prepared from a 1% TbS/HdA complex stock solution loaded with 10% drug. The particles start to aggregate at ∼0.3 mol L^{-1} concentration and finally precipitate at the concentrations of ∼0.5 mol L^{-1}. The drug-loaded particles were more salt resistant. This effect is comparable to that seen with liposomes containing cholesterol. The observed stability of particles in salt solution is surprising, given that the negative ζ-potential would suggest ionic stabilization. However, the lack of aggregation and precipitation of particles up to 0.2 mol L^{-1} indicates that the poloxamer chains, which form the particle corona, have significant steric stabilization effects. Figure 6b shows that the light transmission decreases with increasing particle concentration, while the conductivity remains nearly constant. Based on the data, we conclude that the particles are stable at a pH of 7.4 and a temperature of 25 °C. These results are consistent with the earlier reports on poloxamer-stabilized fatty acid/PE complex nanoparticles.[26]

Incorporation and Release of Compounds. Pyrene was used as a model hydrophobic compound in the complexes because steady-state fluorescence measurements on pyrene-doped complexes provide information about its location in the lamellar structures of the complex. Due to $\pi-\pi^*$ transition, the

https://doi.org/10.1021/acsomega.4c09105
ACS Omega 2024, 9, 50766−50773

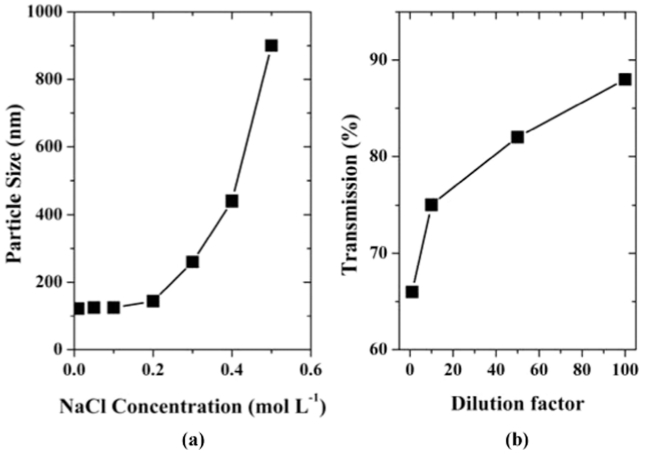

Figure 6. Stability of TbS/HdA core−shell lamellosomes against ionic concentration and dilution stress. (a) Change in the particle size with respect to increasing NaCl concentration. (b) Decrease in transmitted light with increasing lamellosome concentration. The data are a mean of 3 separate experiments, and the relative standard deviation of measurement was less than 30%.

emission spectrum of the monomer pyrene exhibits five peaks (labeled I to V) between 370 and 400 nm with peak I at 372 nm and peak III at 383 nm, which are well resolved. The ratio of peak intensity (I_I/I_{III}) gives information about the polarity of the environment around the pyrene molecule. The excitation spectra show no evidence of aggregation in fluorophore and monomer emission, which is notably higher in mesophases. There is minimal structure visible in excimer peaks, possibly around pH 7.0, where a slight shoulder at around 515 nm is observed. In the TbS/HdA complex, the I_I/I_{III} ratio of the pyrene is 0.69, suggesting that the surroundings of the pyrene are nonpolar, i.e., pyrene is located in hydrophobic HdA domains. This possibility is reinforced by the lack of structure in excimer emission, which is likely due to increased microviscosity. The lamellosome particles were observed under a confocal microscope. Dilaurylcarboxyfluorescein was used as the model dye for the measurements. The confocal microscopy image is shown in Figure 7. The particles appeared as fluorescent dots less than 1.0 μm in size, which correspond to the AFM images. The study conceptually proves the point that TbS/HdA lamellosomes can load hydrophobic drugs.

Having proved the loading of a model compound, the lamellosome formulation was loaded with DxM. It was possible

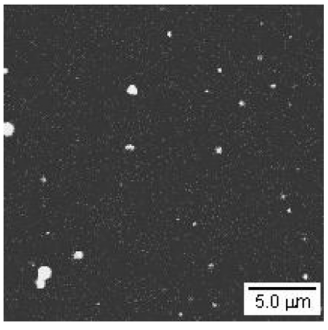

Figure 7. Confocal microscopy image of dilaurylcarboxyfluorescein-loaded lamellosomes. Larger fluorescent dots are observed due to the sample preparation method, i.e., the concentration of the lamellosome sample by centrifugation at 3000*g* and redispersion.

to load up to 1% (w/w) of the TbS/HdA complex without any evidence of DxM crystallization (as observed under a polarized light microscope). The unexpected low loading of the hydrophobic drug, DxM, with a log *P* value of 1.86 may be due to its high melting point (262−264 °C). Propylene glycol assisted in the loading of DxM by reducing the T_g. It was selected, as it is widely used in commercial eye drop preparations. The release profiles of the two drugs (TbS and DxM) present in the lamellosomes were then followed using the procedure described in the Experimental Section. A graph was plotted between the percent cumulative drug release and time (Figure 8). An assessment of filter compatibility in terms of the

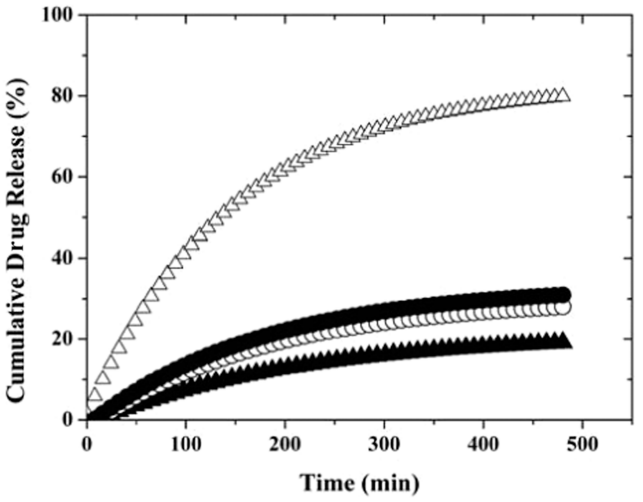

Figure 8. Release profile of DxM (triangles) and TbS (circles) from the lamellosomes. Open legends: Ethanolic release medium; solid legends: buffer release medium. The release was done in triplicate. The relative standard deviation was less than 30%.

binding of the active to the membrane was done to ensure that the membrane material is suitable for use with the two drugs. The value of the diffusional release exponent (n) was calculated by fitting the power law to the curve. The value of n was determined to be ~0.7 ($0.5 < n < 1$), which is indicative of non-Fickian diffusion. The release of TbS followed Fickian ($n = 0.5$) kinetics.[27] Thus, we can say that not only the concentration dependence but also the affinity of DxM to the HdA palisade govern the release. The release of DxM was enhanced when ethanol was included in the release medium. Increased solubility of DxM in ethanolic solution allows easy diffusion out of the complex and into the receptor-cell. Maintaining sink conditions in the dissolution media is one of the criteria for a robust dissolution testing method. Additionally, ethanol partitions in the HdA palisade, thereby increasing the fluidity of the alkyl chains. Though the release profile of TbS remained the same in ethanol, the profile of DxM changed from non-Fickian to Fickian. The release rates of TbS and DxM reversed because the solubility of TbS was not as impacted as DxM. This study established the loading and release of the pharmaceutically relevant combination of drugs from the lamellosomes, thus suggesting potential for sustained combination drug delivery for improved therapy.

CONCLUSIONS

TbS complexes with HdA due to electrostatic interaction and forms lamellar structures. It also contains other periodically

https://doi.org/10.1021/acsomega.4c09105
ACS Omega 2024, 9, 50766−50773

dispersed mesophases, which is confirmed by SAXS and DSC measurements. These can be then dispersed into stable nanoparticles using Poloxamer without loss of a lamellar structure in the core. The lamellosome nanoparticles are composed of TbS/HdA complex mesophases surrounded by a poloxamer corona, which helps stabilization of particles as a result of steric effects. The TbS/HdA lamellosomes can be loaded with hydrophobic compounds, thus making lamellosomes of TbS a multidrug cargo. This paper presents a new drug delivery system for Tbs/DxM, providing physicians with an option of a fixed dose combination of these two drugs that can improve the treatment modality after ocular surgery by potentially improving the antibacterial efficacy and controlling inflammation.

AUTHOR INFORMATION

Corresponding Author

Ajay J. Khopade − *Sun Pharma Advanced Research Centre, Vadodara 390020 Gujarat, India;* orcid.org/0000-0003-3519-7731; Phone: +91 265 6615500; Email: ajay.khopade@sunpharma.com; Fax: +91 265 2354897

Author

Nitin Chitranshi − *Department of Clinical Medicine, Macquarie University, Sydney, NSW 2109, Australia*

Complete contact information is available at: https://pubs.acs.org/10.1021/acsomega.4c09105

Author Contributions

A.J.K.: Writing—original draft, methodology, investigation. N.C.: Data curation, writing, formatting.

Notes

The authors declare no competing financial interest.

ACKNOWLEDGMENTS

A.J.K. thanks Anne Heilig, Frau Zenke, and Rina Pitschke for technical assistance and Late Prof. Mohwald for offering invitation to work within MPIKG. This work was supported by an AvH fellowship to A.J.K.

REFERENCES

(1) Antonietti, M.; Conrad, J.; Thunemann, A. F. Polyelectrolyte-surfactant complexes - a new type of solid, mesomorphous material. *Macromolecules* **1994**, *27* (21), 6007−6011.

(2) Langevin, D. Complexation of oppositely charged polyelectrolytes and surfactants in aqueous solutions-A review. *Adv. Colloid Interface Sci.* **2009**, *147*−*148*, 170−177.

(3) Weiss, A. M.; Lopez, M. A., II; Rawe, B. W.; Manna, S.; Chen, Q.; Mulder, E. J.; Rowan, S. J.; Esser-Kahn, A. P. Understanding How Cationic Polymers' Properties Inform Toxic or Immunogenic Responses via Parametric Analysis. *Macromolecules* **2023**, *56* (18), 7286−7299.

(4) Thünemann, A. F.; General, S. Poly(ethylene imine) n-Alkyl Carboxylate Complexes. *Langmuir* **2000**, *16*, 9634−9638.

(5) Dezanet, C.; Kempf, J.; Mingeot-Leclercq, M. P.; Décout, J. L. Amphiphilic Aminoglycosides as Medicinal Agents. *Int. J. Mol. Sci.* **2020**, *21* (19), 7411.

(6) Jezowska-Bojczuk, M.; Karaczyn, A.; Kozlowski, H. Copper(II) binding to tobramycin: potentiometric and spectroscopic studies. *Carbohydr. Res.* **1998**, *313*, 265−269.

(7) Khopade, A. J.; Arulsudar, N.; Khopade, S. A.; Hartmann, J. Ultrathin antibiotic walled microcapsules. *Biomacromolecules* **2005**, *6*, 229−234.

(8) Khopade, A. J.; Arulsudar, N.; Khopade, S. A.; Knocke, R.; Hartmann, J.; Mohwald, H. From ultrathin capsules to biaqueous vesicles. *Biomacromolecules* **2005**, *6*, 3433−3439.

(9) Bulitta, J. B.; Ly, N. S.; Landersdorfer, C. B.; Wanigaratne, N. A.; Velkov, T.; Yadav, R.; Oliver, A.; Martin, L.; Shin, B. S.; Forrest, A.; Tsuji, B. T. Two Mechanisms of Killing of Pseudomonas aeruginosa by Tobramycin Assessed at Multiple Inocula via Mechanism-Based Modeling. *Antimicrob. Agents Chemother.* **2015**, *59* (4), 2315−2327.

(10) Barauskas, J.; Johnsson, M.; Tiberg, F. Self-Assembled Lipid Superstructures: Beyond Vesicles and Liposomes. *Nano Lett.* **2005**, *5* (8), 1615−1619.

(11) Thünemann, A. F. Polyelectrolyte-surfactant complexes (synthesis, structure and materials aspects). *Prog. Polym. Sci.* **2002**, *27*, 1473−1572.

(12) P Desbois, A. Potential applications of antimicrobial fatty acids in medicine, agriculture and other industries. *Recent Pat. Antiinfect. Drug Discovery* **2012**, *7* (2), 111−122.

(13) Rosalia, M.; Enrica, C.; 1 Erika, M. T.; Rossella, D.; Ida, G.; Bice, C.; Silvia, P. Tobramycin Nanoantibiotics and Their Advantages: A Minireview. *Int. J. Mol. Sci.* **2022**, *23* (22), 14080.

(14) Mingeot-Leclercq, M. P.; Tulkens, P. M. Aminoglycosides: nephrotoxicity. *Antimicrob. Agents Chemother.* **1999**, *43*, 1003−1012.

(15) Mingeot-Leclercq, M. P.; Brasseur, R.; Schanck, A. Molecular parameters involved in aminoglycosides nephrotoxicity. *J. Toxicol. Environ. Health* **1995**, *44*, 263−300.

(16) Engel, L. S.; Callegan, M. C.; Hobden, J. A.; Reidy, J. J.; Hill, J. M.; O'Callaghan, R. J. Effectiveness of specific antibiotic/steroid combinations for therapy of experimental Pseudomonas aeruginosa keratitis. *Curr. Eye Res.* **1995**, *14* (3), 229−234.

(17) Wu, Y. L.; Scott, E. M.; Po, A. L. W.; Tariq, V. N. Ability of azlocillin and tobramycin in combination to delay or prevent resistance development in Pseudomonas aeruginosa. *J. Antimicrob. Chemother.* **1999**, *44*, 389−392.

(18) Russell, E. J.; Sutherland, R. Activity of amoxycillin against enterococci and synergism with aminoglycoside antibiotics. *J. Med. Microbiol.* **1975**, *8*, 1−10.

(19) Jiang, L.; Suri, A. K.; Patel, D. J. Saccharide-RNA recognition in an antibiotic-RNA aptamer complex. *Chem. Biol.* **1997**, *4*, 35−50.

(20) Shelley, S. A.; Paciga, J. E.; Balis, J. U. Lung surfactant phospholipids in different animal species. *Lipids* **1984**, *19*, 857−862.

(21) Khopade, A. J.; Shenoy, D. B.; Khopade, S. A.; Jain, N. K. Phase structures of a hydrated anionic phospholipid composition containing cationic dendrimers and pegylated lipids. *Langmuir* **2004**, *20*, 7368−7373.

(22) Pandit, S. A.; Bostick, D.; Berkowitz, M. L. Complexation of phosphatidylcholine lipids with cholesterol. *Biophys. J.* **2004**, *86*, 1345−1356.

(23) Angelov, B.; Angelova, A.; Ollivon, M.; Bourgaux, C.; Campitelli, A. Diamond-type lipid cubic phase with large water channels. *J. Am. Chem. Soc.* **2003**, *125*, 7188−7189.

(24) Blandamer, M. J.; Briggs, B.; Cullis, P. M.; Engberts, J. B. F. N.; Kacperska, A. Vesicle-surfactant interactions - effects of added surfactants on the gel to liquid-crystal transition for 2 vesicular systems. *J. Chem. Soc., Faraday Trans.* **1995**, *91*, 4275−4278.

(25) Gabizon, A.; Martin, F. Polyethylene glycol-coated (pegylated) liposomal doxorubicin. Rationale for use in solid tumours. *Drugs* **1997**, *54* (4), 15−21.

(26) Thünemann, A. F.; General, S. Nanoparticles of a polyelectrolyte−fatty acid complex: carriers for Q10 and triiodothyronine. *J. Controlled Release* **2001**, *75*, 237−247.

(27) Peppas, N. A.; Brannon-Peppas, L. Water diffusion and sorption in amorphous macromolecular systems and foods. *J. Food Eng.* **1994**, *22*, 189−210.

https://doi.org/10.1021/acsomega.4c09105
ACS Omega 2024, 9, 50766−50773